Quenching-free fluorescence signal from plastic-fibres in proton dosimetry: understanding the influence of erenkov radiation

Christensen, Jeppe Brage; Almhagen, Erik; Nyström, Håkan; Andersen, Claus E.

Published in:
Physics in Medicine and Biology

Link to article, DOI:
10.1088/1361-6560/aaafad

Publication date:
2018

Document Version
Peer reviewed version

Quenching-free fluorescence signal from plastic-fibres in proton dosimetry: Understanding the influence of Čerenkov radiation

Jeppe Brage Christensen[1]†, Erik Almhagen[2,3], Håkan Nyström[3] and Claus E. Andersen[1]

[1]Department of Nuclear Technologies, Technical University of Denmark, Roskilde, Denmark

[2]Medical Radiation Sciences, Department of Immunology, Genetics and Pathology, Uppsala University, Uppsala, Sweden

[3]The Skandion Clinic, Uppsala, Sweden

Abstract.

Photons emitted in optical fibres under proton irradiations have been attributed to be both entirely Čerenkov radiation or to be light consisting of fluorescence with a substantial amount of Čerenkov radiation. The source of the light emission is assessed in order to understand why the signal from optical fibres irradiated with protons reportedly is quenching-free.

The present study uses the directional emittance of Čerenkov photons in 12 MeV and 20 MeV electron beams to validate a Monte Carlo model for simulating the emittance and transmission of Čerenkov radiation in optical fibres.

We show, that less than 0.01 Čerenkov photons are emitted and guided per 225 MeV proton penetrating the optical fibre, and that the Čerenkov signal in the optical fibre is completely negligible at the Bragg peak. Furthermore, by taking the emittance and guidance of both fluorescence and Čerenkov photons into account, it becomes evident that the reported quenching-free signal in PMMA-based optical fibres during proton irradiations is fluorescence.

1. Introduction

Dosimetry with fibre-coupled organic scintillators is known to benefit from near water-equivalence, high spatial resolution, and good energy independence (Beddar et al. 1992*b*, Beddar et al. 1992*c*, De Boer et al. 1993). The temperature dependent light output (Wootton & Beddar 2013, Buranurak et al. 2013) and stem effect (Marckmann et al. 2006, Archambault et al. 2006, Therriault-Proulx et al. 2011, Therriault-Proulx et al. 2013) can be accounted for in different ways. Nonetheless, the non-linear response exhibited by organic scintillators exposed to particles with a high linear energy transfer (LET) remains challenging and the underlying mechanisms are poorly understood. This

† To whom correspondence should be addressed (jepb@dtu.dk)

signal-reduction, termed ionization quenching, is often corrected by applying the semi-empirical formula developed by Birks (1951), but a recent study (Boivin et al. 2016) questions the applicability of the correction-method in low-energy photon beams which therefore motivates different approaches.

An attempt to circumvent the quenching issue was performed as a bare optical fibre was irradiated in a 180 MeV proton beam (Jang et al. 2012). The resulting signal resembled the reference depth-dose measured with an ionization chamber perfectly without any LET-dependent signal reduction, i.e. quenching-free. However, the signal in the optical fibre was at first entirely attributed to originate from Čerenkov radiation rather than fluorescence.

Čerenkov radiation, the emission of optical photons by a charged particle travelling through a dielectric medium with an energy above a material-dependent threshold, differs from fluorescence by having a characteristic emission angle depending on the kinetic energy and material (Beddar et al. 1992*a*, Jelley 1958). Consequently, the measurement of Čerenkov photons with an optical fibre is angular dependent contrary to the isotropic emission of fluorescence.

The interpretation of the optical signal to be entirely Čerenkov radiation was partly corrected by Darafsheh et al. (2016), who concluded that the signal mainly consists of fluorescence but also to be heavily *Čerenkov contaminated*.

A deeper understanding of the fluorescence and Čerenkov radiation is of interest since it finds several applications in radiation therapy dosimetry; Glaser et al. (2013) used Čerenkov emission in water to obtain accurate dose profiles in megavoltage X-ray photon beams, while Helo et al. (2014) developed a quality assurance method using Čerenkov radiation in water tank exposed to therapeutic electron beams. Helo et al. (2014) suggest to image the Čerenkov Bragg peak following proton therapy. Demers et al. (2013), Jarvis et al. (2014), and Lin et al. (2016) investigated the possibilities of tomography and sensing tumours during radiotherapy using Čerenkov excited fluorescence. However, the main emphasis on this work is to understand and utilize the quenching-free signal reported in Jang et al. (2012) as optical fibres are irradiated with protons.

Protons at clinically relevant energies are below the Čerenkov energy threshold in water and plastic-like materials, but give rise to Čerenkov radiation as secondary particles are liberated via Coulomb interactions, by production of positron and electron emitting isotopes, and via interactions where the proton transfers energy to charged or uncharged particles (Helo et al. 2014). The Čerenkov radiation following the said processes in a proton beam exhibits a broad angular distribution due to the particle scattering and Čerenkov radiation following isotropic decays. The angular distribution makes it challenging to measure the emitted optical Čerenkov photons using e.g. an optical fibre since the majority of the emitted optical photons will be absorbed in the optical fibre rather than guided to a photomultipler tube (PMT).

The number of Čerenkov photons per primary in an electron beam generally exceeds that of a proton beam by more than an order of magnitude (Glaser et al. 2014) for water

and plastic-materials. Additionally, the emittance of Čerenkov photons in electron beams has a narrower angular distribution than in proton beams which makes the Čerenkov photons in electron beams easier to measure using an optical fibre with a limited acceptance angle.

The present study utilizes the relative directional emittance of Čerenkov photons in 12 MeV and 20 MeV electron beams to validate a Monte Carlo model for the emittance and transmission of Čerenkov photons in optical fibres. The model is validated against experimental results obtained in therapeutic electron beams. The Monte Carlo implementation is subsequently used to investigate Čerenkov radiation and fluorescence in water and optical fibres exposed to proton beams, with emphasis on the number of fluorescence and Čerenkov photons emitted within the acceptance cone of the fibre per primary particle. The Monte Carlo simulations of fluorescence and Čerenkov radiation in a proton beam is eventually compared to the experimental results.

2. Materials and methods

2.1. Theory

Čerenkov radiation was first observed by Čerenkov (1934), explained theoretically by Frank & Tamm (1937), and is characterized by optical photons emitted by charged particles exceeding the phase velocity of light in a dielectric medium. The refractive index-dependent energy threshold is given as

$$E_{\mathrm{TH}} = m_0 c^2 \left(\frac{1}{\sqrt{1 - n^{-2}}} - 1 \right) \tag{1}$$

for a particle of rest-mass m_0, where n is the average refractive index of the dielectric material, and c the speed of light in vacuum (Jelley 1958). Consequently, the energy threshold for electrons in poly(methyl methacrylate) (PMMA) ($n = 1.49$) and water ($n = 1.33$) is 178 keV and 264 keV respectively. As protons are ~ 1836 times heavier than electrons, the Čerenkov energy thresholds for protons in PMMA and water are above clinically relevant energies. However, protons above 80 MeV in PMMA and 115 MeV in water (Glaser et al. 2014) may liberate electrons above the Čerenkov energy threshold and at lower energies via nuclear interactions.

The number $\mathrm{d}N$ of optical photons emitted by an electron with energy E within the spectral region defined by wavelengths $\lambda_1 < \lambda_2$, traversing a distance $\mathrm{d}x$, is given by the Frank-Tamm formula (Jelley 1958) as

$$\frac{\mathrm{d}N}{\mathrm{d}x} = 2\pi\alpha \left(\frac{1}{\lambda_1} - \frac{1}{\lambda_2} \right) \sin^2 \theta, \tag{2}$$

where $\alpha = 1/137$ is the fine structure constant, and

$$\theta = \arccos\left(\frac{1}{\beta n} \right), \qquad \text{for} \quad \beta = \sqrt{1 - \left(\frac{m_0 c^2}{E + m_0 c^2} \right)^2}, \tag{3}$$

is the angle at which the optical Čerenkov photons are emitted relative to the direction of the electron. The angular dependency is crucial for the present case where the light must be guided through optical fibres requiring the emitted optical photons to be within the acceptance cone of the fibre in question. The spectral intensity distribution in eq. (2) and the angular dependency in eq. (3) make it feasible to experimentally confirm the presence of Čerenkov radiation.

2.2. Experimental setup

The study uses a 15 m optical fibre with 480 µm diameter PMMA core and fluorinated polymer ($n = 1.40$) as cladding with a 500 µm outer diameter (GH-4001-P, Mitsubishi Rayon Co., Ltd., Japan). A black polyethylene fibre-jacket protected the cladding and core, with an outer diameter of 1000 µm, from external light.

The optical fibre was irradiated with 12 MeV and 20 MeV electrons at a medical linac (TrueBeam, Varian Medical Systems, USA) where the attached SMA-connector was connected to an ME-40 device with two PMTs (Beierholm et al. 2014). An in-house build x-ray source (Andersen et al. 2003) was used to irradiate the bare optical fibre with 50 kVp photons.

Optical spectra of the light transmitted through the fibre under irradiations with photons and electrons were obtained with a monochromator (Model 77250, Oriel Instruments, USA) placed outside the treatment room. The acquisition time for all spectra was set to 15 mins to compensate for the low optical signal as the fibre was irradiated with 50 kVp X-ray, and kept for consistency during electron irradiations. The monochromator was connected to a photomultiplier tube (MP-982, PerkinElmer, USA) coupled to a laptop with data acquisition software. Measurements of the optical spectra and the optical signal as a function of gantry angle are conducted with the fibres suspended in air whereas the depth curves are simulated and measured in water.

A 180 MeV spot-scanning proton beam (Proteus 235, IBA, Belgium) at the Skandion Clinic, Uppsala, was used to irradiate the optical fibre placed in a water phantom (Blue Phantom, IBA Dosimetry, Germany) with a 41×41 spots in a 10 cm $\times$ 10 cm field. A 180 MeV spot had a full width at half maximum (FWHM) of 9.4 mm and each spot was delivered in approximately 22 ms. An ionization chamber (Bragg Peak Ionization Chamber No. 34070, PTW Freiburg, Germany) was used to measure the reference depth-dose curve.

The 180 MeV energy is chosen for the experimental irradiations for comparisons with Jang et al. (2012) and Darafsheh et al. (2016) whereas 225 MeV, with the most Čerenkov radiation per primary, is chosen for the simulations to investigate the so-called Čerenkov contamination referred to by Darafsheh et al. (2016).

2.2.1. Monte Carlo parameters. The number of emitted fluorescence photons per energy in the optical fibre is required as an input in GEANT4. The number is estimated by comparing the outputs of a fibre-coupled scintillator irradiated with same doses in

(i) a point in the scintillator and (ii) in the optical fibre 1 cm from the scintillator, giving a negligible difference in the fibre transmission lengths. The irradiations took place in a ^{60}Co source (Terabalt T100, UJP Praha, Czech Republic), where the fiber-coupled scintillator was placed at angle relative to the ^{60}Co beam direction to favour the absorption of Čerenkov photons in the optical fibre rather than guidance. The scintillator (BCF-60, Saint-Gobain, France) yields 7100 photons/MeV according to the manufacturer which allowed an estimation of the number of fluorescence photons per deposited energy. The estimate was subsequently used as a lower threshold of the amount of fluorescence photons being guided in the optical fibre in subsection 3.5.

A fibre-subtraction method as described in Jang et al. (2012) was used to validate the Monte Carlo code against experimentally obtained results. The setup is sketched in figure 1 where the Čerenkov radiation in 5 cm of the irradiation field is estimated by subtracting the signal from one fibre from another. The two bare optical fibres are each connected to a PMT in the ME-40 setup with same gain.

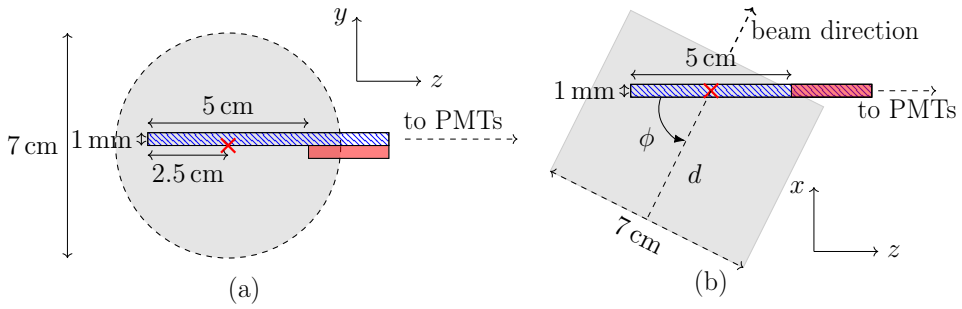

Figure 1. The fibre-subtraction method used to validate the Monte Carlo implementation where the 7 cm diameter radiation field is (a) perpendicular to the two fibres and (b) rotated an angle ϕ. Fibre 1 (hatched rectangle) and fibre 2 (filled rectangle) are separated with a 5 cm distance and each connected to a photomultiplier tube. The top-view in (b) shows the source-to-fibre distance d where the beam is rotated an angle ϕ relative to the fibres.

2.3. Monte Carlo simulations

The dose deposition, spatial distribution, and guidance of Čerenkov photons in water and the optical fibres were investigated with the Monte Carlo software GEANT4 10.2 (Agostinelli et al. 2003). The optical Čerenkov photons were generated in the waveband 380 nm to 700 nm where the refractive indices for water, PMMA, and fluorinated polyethylene (cladding material) were set to be spectrally constant as 1.33, 1.49, and 1.40 respectively. Fluorescence photons were generated in the same waveband as Čerenkov radiation with a spectral distribution in the optical fibre as in De Boer et al. (1993). The number of emitted fluorescence photons per energy was for this particular optical fibre estimated to be 340 photons/MeV cf. the procedure in subsection 2.2.

The standard electromagnetic package with `option4` was used along with the `QGSP_BIC` hadron physics package. The GEANT4 implementation of the simulated

emission and scoring of Čerenkov photons was compared to and validated against results in Glaser et al. (2014) for photons, electrons, and protons in water. 10^8 primary particles were used in the case of electron beams, whereas an order of 10^9 protons was required due low number of emitted Čerenkov photons per proton in the optical fibre. Čerenkov and fluorescence emission profiles were simulated in a $1\,\mathrm{m} \times 1\,\mathrm{m} \times 1\,\mathrm{m}$ water tank where the primary particles were sampled uniformly from a monoenergetic circular source with radius 2 cm placed in the middle of the tank.

The emittance and guidance of Čerenkov photons in the Monte Carlo model of the optical fibre is validated against experimental data in subsection 3.4.

3. Results

3.1. Angular dependency

The Čerenkov emission angle in the optical fibre is investigated experimentally by irradiating optical fibres at different angles with 20 MeV electrons. The PMT signal as a function of gantry angle, with the angle defined as in figure 1(b), is shown in figure 2(a). The angular Čerenkov radiation peak matches the theoretical emission angle in the fibre-core (PMMA), which confirms that fluorescence is negligible relative to the Čerenkov radiation for electron beams, if the irradiation angle is chosen properly to favour the Čerenkov radiation.

3.2. Spectral distributions

Spectral distributions of the photons generated in the optical fibres exposed to electron beams are acquired at two irradiation angles as defined in figure 2(b); one optimized for guidance of the Čerenkov radiation and one where the guidance is minimal cf. eq. (3). The Čerenkov emission angle for electrons at infinite energies ($\theta \simeq \arccos n^{-1}$) is 47.8° in PMMA, i.e. in the fibre core.

Thus, the angle between the beam and optical fibre, ϕ as chosen as in figure 1(b), is set to $\phi = 45°$ to obtain a Čerenkov spectrum, and $\phi = 135°$ for a fluorescence spectrum. The two irradiation angles are chosen to ensure that the same length of fibre is irradiated in both electron measurements, which gives rise to the same fluorescence signal. For comparison, another fluorescence spectrum was obtained by irradiating the optical fibre in a 50 kVp X-ray source, i.e. well below the Čerenkov-threshold.

3.3. Čerenkov radiation in electron beams

3.3.1. Čerenkov radiation distribution. Studies (Helo et al. 2014, Glaser et al. 2014) report a small depth-shift between the dose and emission of optical Čerenkov photons as a function of the depth in electron beams as shown in figure 3(a).

The kinetic energy of a 20 MeV electron beam in water is scored along the central axis in figure 3(b) with GEANT4 for reference, where the Čerenkov emission angle in

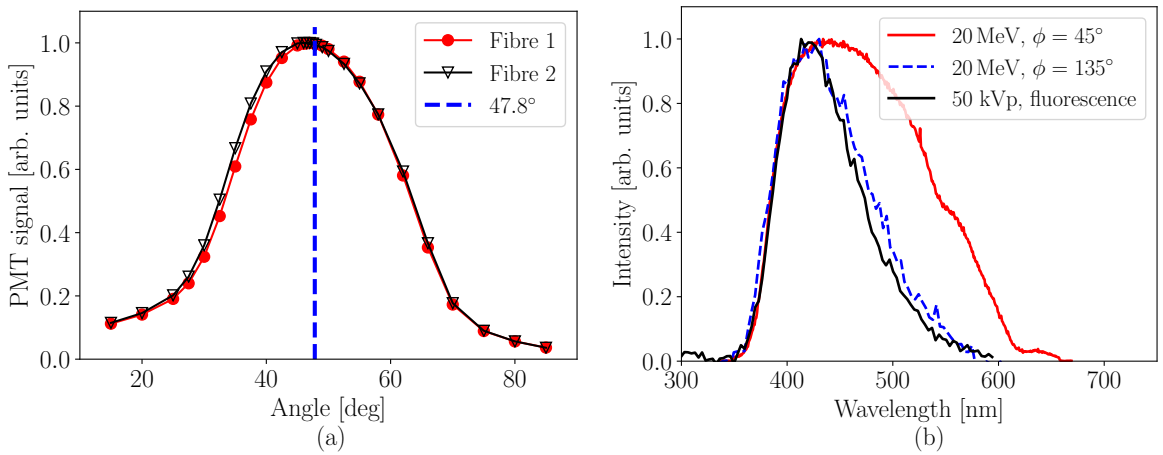

Figure 2. (a) The PMT signal as a function of gantry angle as optical fibres are irradiated with 20 MeV electrons along with the theoretical emission angle in the fibre core (dashed line). (b) The fluorescence spectrum of the optical fibre obtained with a 50 kVp X-ray source, along with spectra from irradiations using 20 MeV electrons at $\phi = 45°$ (Čerenkov dominated spectrum) and $\phi = 135°$ (fluorescence spectrum) with angles chosen as in figure 1(b).

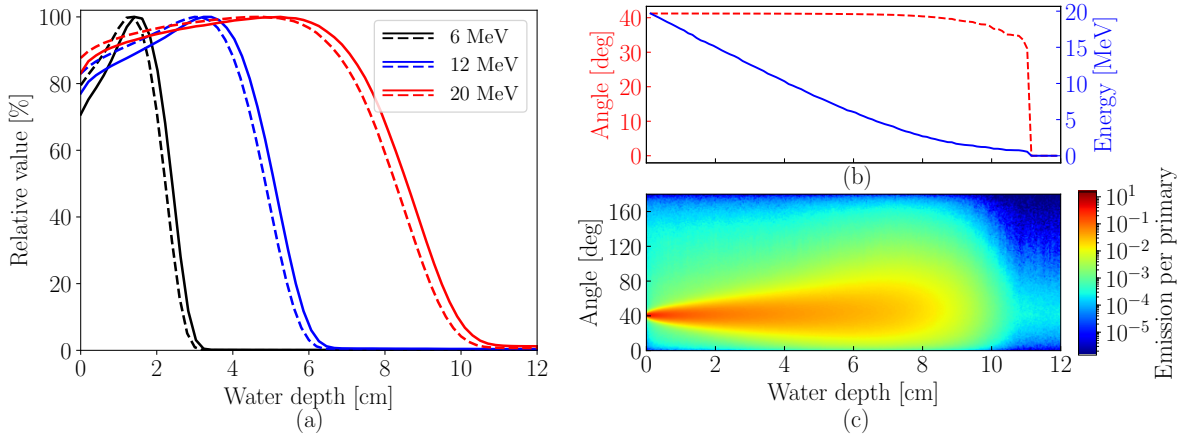

Figure 3. GEANT4 simulations of electrons in water. (a) The distribution of dose (solid lines) and emission of Čerenkov photons (dashed lines) for three energies in water. (b) The kinetic energy (solid line) scored along the central axis of a 20 MeV electron beam. The Čerenkov emission angle (dashed line) is plotted as a function of the energy for comparison. (c) The emission angle scored relative to the beam direction.

eq. (3) is plotted as a function of the energy, i.e. the emission angle relative to the beam direction if no interaction would occur. Figure 3(c) shows the actual angles at which Čerenkov photons are emitted relative to the beam direction scored with a 500×500 grid in water for 20 MeV electrons. The majority of the Čerenkov photons are emitted an angle around 41.2° as predicted by eq. (3).

3.4. Measured depth-profile of Čerenkov radiation

The emission of Čerenkov photons as a function of the water depth is investigated with the fibre-subtraction method sketched in figures 1(a)–(b) with an irradiation angle of $\phi = 45°$. The Čerenkov radiation in the 5 cm difference region was estimated by subtracting the smaller PMT signal from the larger. An identical setup was implemented in GEANT4 where only the Čerenkov radiation is scored. Depth-curves of the normalized signal difference were now experimentally obtained by mechanically moving the fibres through the water phantom, and equivalently in the Monte Carlo code with a photon counter at the fibre end. The experimental results and Monte Carlo simulations are shown in figure 4 for 12 MeV and 20 MeV electrons in water.

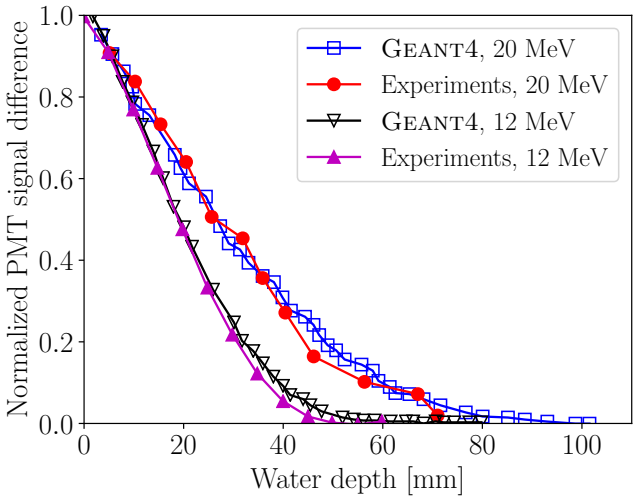

Figure 4. The fibre-subtraction method applied to experiments and Monte Carlo simulations for 12 MeV and 20 MeV electrons. The fibres were irradiated at an angle $\phi = 45°$ in a water phantom.

3.5. Čerenkov radiation and fluorescence in clinical proton beams

The emittance of optical Čerenkov photons in a proton beam is more complex to relate to the dose-profile than for electron beams. The depth profile of both dose and Čerenkov radiation is shown in figure 5(a). The Čerenkov radiation is scored in a cylinder with 1.5 cm radius along the axis of a pencil beam.

The first half of the range is dominated by Čerenkov photons emitted by electron liberated by protons (Glaser et al. 2014, Helo et al. 2014) until a point where the protons no longer have energy to liberate electrons above the Čerenkov energy threshold in eq. (1). The angular distribution of emitted Čerenkov photons in water, including the contributions from electron scattering and Čerenkov emission following induced radioisotopes, is shown in figure 5(b).

GEANT4 simulations of Čerenkov radiation and fluorescence as an optical fibre is placed perpendicular to a 225 MeV proton beam are shown in figure 6(a)–(b)

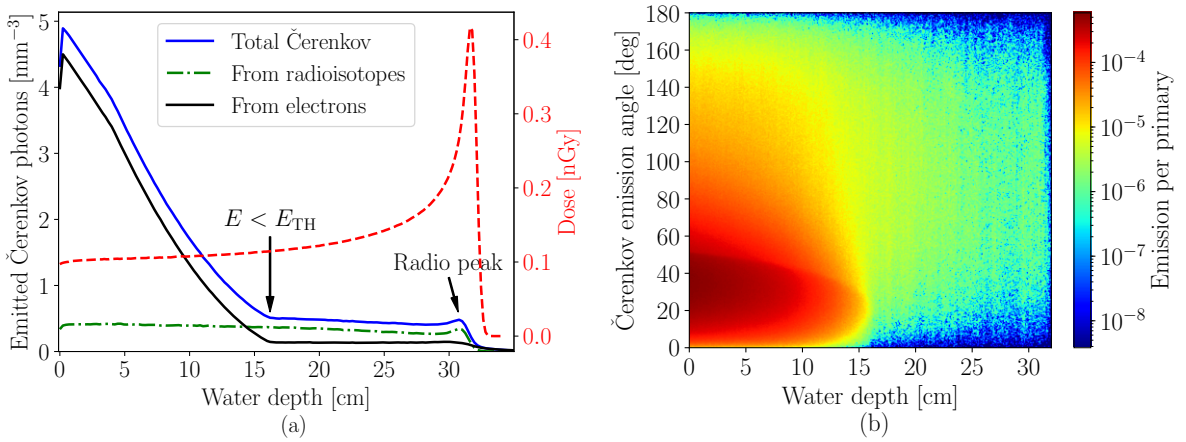

Figure 5. GEANT4 simulations of 225 MeV protons in water. (a) The majority of the Čerenkov radiation arises from liberated electrons with a spatial distribution different from the dose, although a minor radiopeak is observable at the Bragg peak. (b) Angular distribution of the emitted Čerenkov photons scored in a 500×500 grid relative to the beam direction reveals a broader emission distribution than in electron beams.

respectively. The results have been normalized to the number of Čerenkov and fluorescence photons emitted and guided through the optical fibre per proton.

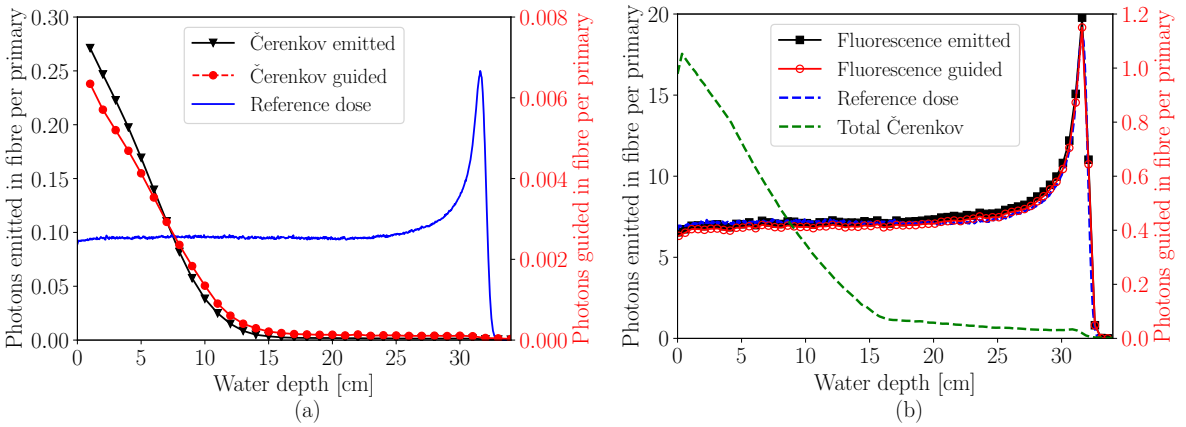

Figure 6. GEANT4 simulations of 225 MeV protons in water. (a) The number of Čerenkov photons emitted and guided in the optical fibre per proton. (b) The number of (isotropically) emitted fluorescence emission per proton emitted and guided in the optical fibre.

3.6. Experimental irradiation of optical fibres with protons

The optical fibres were placed in a water phantom perpendicular to the beam direction (i.e. $\phi = \pi/2$ in figure 1(b)) and irradiated with 180 MeV protons in a 10 cm $\times$ 10 cm field consisting of 41×41 spots. The setup is sketched in figure 7(a) where an optical fibre is placed in the centre of the field but does not extend to the edge. A signal is detected for each of the 41 horizontal scan lines which results in the 41 peaks in figure 7(b). The

4 decreasing peaks to the right correspond to the case, where the beam does not scan directly over the fibre as illustrated in the upper part of figure 7(a).

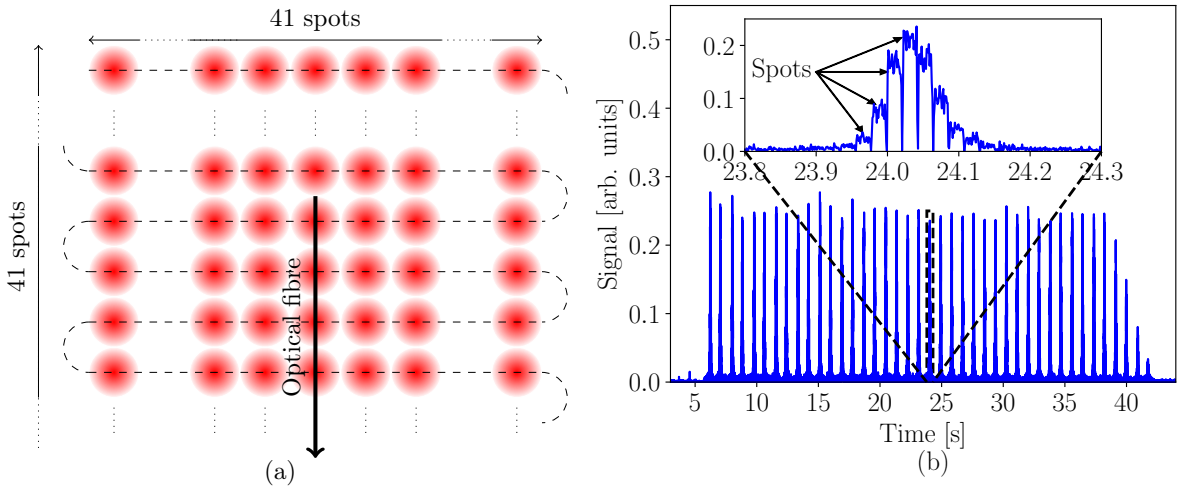

Figure 7. An optical fibre placed orthogonal to the 180 MeV proton beam direction in a water phantom. (a) The scanning pattern with the optical fibre placed in the middle of the field. (b) The signal as the beam scans by the optical fibre in (a) 41 times at 6 cm depth. The close-up shows the deposition of single spots. The signal increases, as the beam approaches the fibre, and subsequently decreases as the beam passed by.

The PMT, with a resolution on the micro-second scale, was able to resolve the delivery of each spot in the vicinity of the fibre as seen in the close-up in figure 7(b). The optical signal as a function of depth is calculated from the scan lines that passed directly over the fibre, i.e. the 37 peaks from left to right in figure 7(b). The response of the optical fibre irradiated with protons at a given depth is calculated in two ways: Firstly by averaging over an integration of each of the 37 peaks and, secondly, by averaging over the signal amplitude of each of the 37 peaks. The results are in figure 8 compared to a reference curve obtained with a Bragg Peak ionization chamber normalized to the entrance value.

4. Discussion

4.1. Optical photons in electron beams

The PMT signal as a function of gantry angle in figure 2(a) indicates, that Čerenkov radiation in the optical fibre might completely dominate fluorescence in electron beams if the irradiation angle is chosen properly. The coinciding spectra obtained in the 50 kVp X-ray source and with 20 MeV electrons ($\phi = 135°$) in figure 2(b) confirm, that the Čerenkov radiation indeed is emitted outside the acceptance cone at such an angle. The fluorescence spectrum is in agreement with results published in De Boer et al. (1993). Hence, the spectrum obtained in the 20 MeV electron linac at $\phi = 45°$ is the result of a Čerenkov spectrum convolved with the transmission profile of the optical fibre where

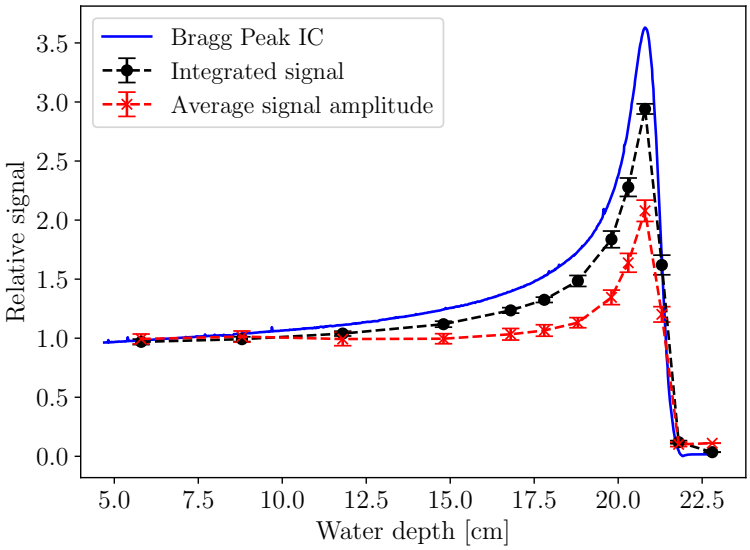

Figure 8. The integrated signal from for each depth measurements resembles the reference depth-dose curve obtained with an ionization chamber.

no photons below 350 nm are transmitted in PMMA.

The spectra are for simplicity scaled to their respective maximum value but the electron spectra were acquired with same dose-rates and same length of irradiated fibre; the actual intensity of the Čerenkov spectrum ($\phi = 45°$) is of the order of 15 times more intense than the fluorescence spectrum obtained at $\phi = 135°$ and thus indeed confirms the presence of Čerenkov radiation.

4.1.1. Monte Carlo validation. The effective signal estimated from the fibre-subtraction method for $\phi = 45°$ is dominated by Čerenkov radiation as shown in figures 2(a)–(b). However, according to figure 3(c), the Čerenkov emittance per electron is diminished with almost two orders of magnitude at half the range relative to the entrance for such an angle between fibre and beam. Hence, if the Čerenkov radiation from 20 MeV electrons were to be measured as a function of water depth with an optical fibre placed an angle $\phi \sim 45°$, the Čerenkov signal is expected to be negligible after ~ 8 cm.

The results in figure 4 show good agreements for both 12 MeV and 20 MeV electrons between calculations with the GEANT4 model of the fibres in the water phantom and experimentally measured in the medical linac. The agreements in this critical test validate the Monte Carlo implementation of the fibres and the simulation of emission and transmission of Čerenkov radiation. The Monte Carlo implementation of the optical fibres is henceforth used to investigate Čerenkov radiation in a proton beam in detail which otherwise would not have been feasible.

4.2. Protons

4.2.1. Čerenkov radiation. The GEANT4 simulations of Čerenkov radiation emission in a 225 MeV proton beam in water are shown in figure 5(a)–(b). The overall emission of Čerenkov photons becomes more isotropic as the protons slow down and Čerenkov emission following isotropic decays start to be significant, which in turn makes it challenging to measure the Čerenkov photons with e.g. an optical fibre. Although the secondary electrons above the Čerenkov radiation energy threshold are liberated in a primarily forward direction, the combination of an energy-dependent Čerenkov radiation emission direction and particle scattering yield the broad angular Čerenkov distribution. The angular distribution of emitted Čerenkov photons nonetheless indicates, it may be advantageous to place the optical fibre at an $\approx 30^\circ$ angle relative to the beam direction to guide as much Čerenkov radiation as possible through an optical fibre.

4.2.2. Transition radiation. It should be noted that also transition radiation (Ginzburg & Frank 1946) gives rise to optical photons in the fibre due to differing optical properties (Jelley 1958). However, as the intensity of transition radiation is proportional to $\gamma = 1/\sqrt{1-\beta^2}$, the transition radiation in an optical fibre is negligible relative to fluorescence for proton beams at clinical energies, and generally not emitted within the acceptance angle of the fibre (when placed perpendicular to the beam) as the radiation is peaking at an angle γ^{-1} relative to the particle's path (Dolgoshein 1993).

4.2.3. Fluorescence and Čerenkov radiation in optical fibres. The simulations in figure 6(a), using the Monte Carlo implementation of the emission and transmission of Čerenkov radiation validated in an electron linac, indicate the problems related to measurements of Čerenkov radiation in proton beams. Although just less than one Čerenkov photon per proton is emitted in a fibre placed at the entrance, only a fraction of these photons are emitted within the acceptance angle of the optical fibre. The simulation does not take the attenuation of the optical fibre into account and consequently serves as an ideal case.

The number of fluorescence photons emitted in the fibre along with the number of fluorescence photons within the acceptance angle of the fibre per proton is shown in figure 6(b). The fluorescence distribution exhibits, due to its isotropic nature, the same depth-dependence as deposited energy; the ionization quenching is not included in the simulations as the above-mentioned results in Jang et al. (2012) indicate, that quenching is negligible in the PMMA-based fibre. A comparison between the figures 6(a)–(b) gives, that the number of fluorescence photons within the acceptance angle of the optical fibre per proton is more than an order of magnitude larger than that of Čerenkov radiation. In the case of a 225 MeV proton beam, Čerenkov radiation is completely negligible after ~ 14 cm. Hence, the optical photon signal measured with a fibre placed perpendicular to a proton beam is largely dominated by fluorescence photons.

These results, based on Monte Carlo implementation of the fibres validated in

known Čerenkov radiation regimes, do not support the hypotheses that the optical signal under proton irradiation is neither (i) solely Čerenkov radiation as in Jang et al. (2012) nor that (ii) Čerenkov radiation is able to *contaminate* the fluorescence signal substantially after 14 cm water depth (see figure 6(a)) in a 225 MeV proton beam as described in Darafsheh et al. (2016).

4.2.4. Experimental results for protons. Generally, it was possible to distinguish between the 8–9 spots closest to the fibre in each scan line as seen in figure 7(b). As one may infer from the close-up in figure 7(b), the FWHM of the signal in a scan line is about 4 spots which corresponds to FWHM $\simeq$ 1 cm at 6 cm water depth with the given number of spots and field size. The actual FWHM = 9.4 mm for the beam at the entrance region for the same energy indicates, that optical fibres may be used to monitor both the spot size and delivery time, which, however, is out of the scope of this work.

The measured Bragg peak in figure 8 is the result of fluorescence, as measured with the monochromator during irradiations with photons below the Čerenkov energy threshold in figure 2, and simulated in figure 6(b). The signal reduction at the Bragg peak was anticipated due to spread of the beam spots with increasing water depth and the 1 mm diameter of the fibre. The interpretation of fluorescence is in agreement with other sources (Peeples et al. 2012, Yamamoto et al. 2018) reporting of a strong correlation between luminescence and dose profile as water is irradiated with photons or protons below the Čerenkov threshold.

4.3. Ionization quenching

The apparently quenching-free curve as a results of a PMMA-based optical fibre irradiated with protons (Jang et al. 2012) may give information about the nature of ionization quenching. In order to understand the quenching-free results, we present two hypotheses based on differences between the optical fibre and traditional organic scintillators.

The emission of light from PMMA-based materials is different from that of polystyrene-based scintillators. Acetone, a ketone which spectroscopically has similarities to the ester in PMMA, has a singlet-singlet transition about three orders of magnitude stronger than its triplet-singlet transition (Becker et al. 1983). Thus, we suggest a possible explanation of the lack of quenching could be the dominating singlet-singlet transition in the optical fibre, although the presence of e.g. O_2 in the fibre core inevitably leads to triplet-singlet transitions.

Another approach to understand the quenching-free results is to consider the number of excited molecules involved in the quenching process. Blanc et al. (1962) developed a general equation to describe the kinetics of the excitation densities, where Birks' formula is a solution to a simplified version of their equation (Birks 1964). The quenching in this formulation consists of terms, where the density of excited molecules

are of power 2 and higher, and thus extremely density-dependent. The low local concentration of excited molecules in PMMA, compared to excitation concentrations in typical scintillator-based materials, consequently results in a much lower (if not negligible) ionization quenching in the optical fibre compared to organic scintillators.

5. Conclusions

The Čerenkov radiation and fluorescence emitted in optical fibres exposed to electron beams was used to establish a foundation, where a Monte Carlo implementation of the emission and transmission of optical photons was validated against experimental data. The simulations of emittance and guidance of optical photons in fibres irradiated with protons indicate, that fluorescence—and not Čerenkov radiation—is responsibly for the optical Bragg peak measured in a 180 MeV proton beam, where the signal reduction relative to the reference dose curve in this work is due to the small spot size relative to the fibre-diameter.

The validated model does not support the hypotheses, that the optical signal in a fibre under proton irradiations is (i) entirely Čerenkov radiation (Jang et al. 2012) nor (ii) severely Čerenkov contaminated (Darafsheh et al. 2016), since neither follows the depth distribution nor spatial extension of Čerenkov distribution and the amount of fluorescence, furthermore, greatly exceeds that of Čerenkov radiation.

The mechanism behind the quenching-free fluorescence signal in optical fibres during proton irradiations still needs to scrutinized further.

Acknowledgments

The work was supported by the Danish Cancer Society. The authors thank Lars René Lindvold, Technical University of Denmark, for stimulating discussions pertaining to luminescence properties and Čerenkov radiation effects in optical fibres.

References

Agostinelli S, Allison J, Amako K a, Apostolakis J, Araujo H, Arce P, Asai M, Axen D, Banerjee S, Barrand G et al. 2003 GEANT4—a simulation toolkit *Nucl. Instrum. Methods A* **506** 250–303.

Andersen C E, Bøtter-Jensen L & Murray A S 2003 A mini X-ray generator as an alternative to a ^{90}Sr/^{90}Y beta source in luminescence dating *Radiat. Meas.* **37** 557–61.

Archambault L, Beddar A S, Gingras L, Roy R & Beaulieu L 2006 Measurement accuracy and Cerenkov removal for high performance, high spatial resolution scintillation dosimetry *Med. Phys.* **33** 128–35.

Becker H G O, Böttcher H, Dietz F, Rehorek D, Roewer G, Schiller K & Timpe H J 1983 *Einführung in die Photochemie* Georg Thieme Verlag Stuttgart, New York.

Beddar A S, Mackie T R & Attix F H 1992*a* Cerenkov light generated in optical fibres and other light pipes irradiated by electron beams *Phys. Med. Biol.* **37** 925–35.

Beddar A S, Mackie T R & Attix F H 1992*b* Water-equivalent plastic scintillation detectors for high-energy beam dosimetry: I. Physical characteristics and theoretical considerations *Phys. Med. Biol.* **37** 1883–900.

Beddar A S, Mackie T R & Attix F H 1992*c* Water-equivalent plastic scintillation detectors for high-energy beam dosimetry: II. Properties and measurements *Phys. Med. Biol.* **37** 1901–13.

Beddar S & Beaulieu L 2016 *Scintillation Dosimetry* CRC Press.

Beierholm A R, Behrens C F & Andersen C E 2014 Dosimetric characterization of the Exradin W1 plastic scintillator detector through comparison with an in-house developed scintillator system *Radiat. Meas.* **69** 50–56.

Birks J B 1951 Scintillations from organic crystals: specific fluorescence and relative response to different radiations *Proceedings of the Physical Society. Section A* **64** 874–77.

Birks J B 1964 *The Theory and Practice of Scintillation Counting: International Series of Monographs in Electronics and Instrumentation* Vol. 27 Elsevier.

Blanc D, Cambou F & de Lafond Y G 1962 Kinetics of the fast component of scintillation in a pure organic medium. Application to anthracene *Comptes rendus de l'Académie des Sciences Paris* **18** 3187–89.

Boivin J, Beddar S, Bonde C, Schmidt D, Culberson W, Guillemette M & Beaulieu L 2016 A systematic characterization of the low-energy photon response of plastic scintillation detectors *Phys. Med. Biol.* **61** 5569–86.

Buranurak S, Andersen C E, Beierholm A R & Lindvold L R 2013 Temperature variations as a source of uncertainty in medical fiber-coupled organic plastic scintillator dosimetry *Radiat. Meas.* **56** 307–311.

Čerenkov P A 1937 Visible radiation produced by electrons moving in a medium with velocities exceeding that of light *Physical Review* **52** 378–79.

Darafsheh A, Taleei R, Kassaee A & Finlay J C 2016 The visible signal responsible for proton therapy dosimetry using bare optical fibers is not Čerenkov radiation *Med. Phys.* **43** 5973–80.

De Boer S F, Beddar A S & Rawlinson J A 1993 Optical filtering and spectral measurements of radiation-induced light in plastic scintillation dosimetry *Phys. Med. Biol.* **38** 945–58.

Demers J L, Davis S C, Zhang R, Gladstone D J & Pogue B W 2013 Čerenkov excited fluorescence tomography using external beam radiation *Optics letters* **38** 1364–1366.

Dolgoshein B 1993 Transition radiation detectors *Nucl. Instrum. Methods A* **326** 434–469.

Frank I & Tamm I 1937 Coherent visible radiation from fast electrons passing through matter *Acad. Sci. USSR* **14** 109–14.

Ginzburg V & Frank I 1946 To the Theory of Transition Radiation *Sov. Phys.* **16** 15.

Glaser A K, Davis S C, Voigt W H, Zhang R, Pogue B W & Gladstone D J 2013 Projection imaging of photon beams using Čerenkov-excited fluorescence *Phys. Med. Biol.* **58** 601–19.

Glaser A K, Zhang R, Gladstone D J & Pogue B W 2014 Optical dosimetry of radiotherapy beams using Čerenkov radiation: the relationship between light emission and dose *Phys. Med. Biol.* **59** 3789–811.

Helo Y, Kacperek A, Rosenberg I, Royle G & Gibson A P 2014 The physics of Čerenkov light production during proton therapy *Phys. Med. Biol.* **59** 7107–23.

Helo Y, Rosenberg I, DSouza D, MacDonald L, Speller R, Royle G & Gibson A P 2014 Imaging Čerenkov emission as a quality assurance tool in electron radiotherapy *Phys. Med. Biol.* **59** 1963–78.

Jang K W, Yoo W J, Shin S H, Shin D & Lee B 2012 Fiber-optic Čerenkov radiation sensor for proton therapy dosimetry *Optics Express* **20** 13907–14.

Jarvis L A, Zhang R, Gladstone D J, Jiang S, Hitchcock W, Friedman O D, Glaser A K, Jermyn M & Pogue B W 2014 Cerenkov video imaging allows for the first visualization of radiation therapy in real time *Int. J. Radiat. Oncol. Biol. Phys.* **89** 61522

Jelley J V 1958 *Čerenkov radiation and its applications* Pergamon.

Lin H, Zhang R, Gunn J R, Esipova T V, Vinogradov S, Gladstone D J, Jarvis L A & Pogue B W 2016 Comparison of Cherenkov excited fluorescence and phosphorescence molecular sensing from tissue with external beam irradiation *Phys. Med. Biol.* **61** 3955–68.

Marckmann C J, Aznar M C, Andersen C E & Bøtter-Jensen L 2006 Influence of the stem effect on radioluminescence signals from optical fibre Al2O3: C dosemeters *Radiat. Prot. Dosim.*

119 363–67.

Peeples J L, Stokely M H, Poorman M C, Magerl M & Wieland B W 2012 Visual observation of boiling in high power liquid target AIP Conference Proceedings **1509** 76–80.

Therriault-Proulx F, Beaulieu L, Archambault L & Beddar S 2013 On the nature of the light produced within PMMA optical light guides in scintillation fiber-optic dosimetry *Phys. Med. Biol.* **58** 2073–84.

Therriault-Proulx F, Beddar S, Briere T M, Archambault L & Beaulieu L 2011 Removing the stem effect when performing Ir-192 HDR brachytherapy in vivo dosimetry using plastic scintillation detectors: A relevant and necessary step *Med. Phys.* **38** 2176–79.

Wootton L & Beddar S 2013 Temperature dependence of BCF plastic scintillation detectors *Phys. Med. Biol.* **58** 2955–67.

Yamamoto S, Koyama S, Yabe T, Komori M, Tada J, Ito S, Toshito T, Hirata Y & Watanabe K 2018 Stability and linearity of luminescence imaging of water during irradiation of proton-beams and X-ray photons lower energy than the Cerenkov light threshold *Nucl. Instrum. Methods A* **803** 48–56